Physica A 188 (1992) 137–157
North-Holland

PHYSICA A

Competition in ramped Turing structures

P. Borckmans[1], A. De Wit[2] and G. Dewel[1]

[1]*Service de Chimie-Physique and* [2]*Centre for Nonlinear Phenomena and Complex Systems, C.P. 231, Université Libre de Bruxelles, 1050 Brussels, Belgium*

Stationary pattern selection and competition in the uniform Brusselator in two (2D) and three (3D) dimensions are reviewed, including reentrant hexagonal and striped zig-zag phases. Influences of linear or chain-like profiles of the pool chemicals on this selection are presented in the form of numerical experiments. The relation with the recent experimental patterns obtained with the CIMA reaction is discussed.

1. Introduction

Turing structures [1] are stationary periodical concentration patterns resulting from a diffusive instability originating from the sole coupling of reaction and diffusion processes [2]. It has been claimed that such a mechanism may have deep biological implications [1–4]. Was the original paper of Turing not entitled "Chemical basis for morphogenesis"? They however remain to be fully vindicated. From another fundamental point of view they may also prove to be important. Indeed they are characterized by an intrinsic wavelength that depends only on the diffusion coefficients, kinetic constants and concentration of some control species and not on some geometrical parameter of the experimental set-up. The experimental 3D chemical patterns may therefore prove to be the first structures far from equilibrium resulting from a true symmetry-breaking process [5, 6].

As was foreseeable, the observation [7–12] of genuine Turing structures in solution chemistry, nearly forty years after their prediction, triggered a wave of renewed experimental and theoretical interest. Hopefully the tremendous corpus of theoretical knowledge that had accumulated may now be put to the test.

To the eye, the similarities between the symmetries of the experimentally observed structures and those predicted from the nonlinear theory for uniform conditions [13–17], are undeniable. In the experimental conditions the system

[1] Senior Research Assistant with the F.N.R.S. (Belgium).
[2] I.R.S.I.A. (Belgium) Fellow.

is however kept under control by feeds through the boundaries that create specific nonuniformities. This led us to try to understand the effects of parameters ramps on the pattern selection problem – the aim of which is summarized in section 2 – in a 2D and 3D chemical system with the aid of intensive numerical simulations. In the third section we first summarize the bifurcation behaviour under uniform conditions for the Brusselator model in large systems, on which our studies are performed. Indeed this bifurcation structure may then be used, in the fourth section, to help us organize the closer to experiments ramped situations.

The properties of the patterns obtained for uniform constraints may however also be of interest in regard of the experimental results in the new CSTR–membrane reactor [11] and also when the applied experimental ramps of concentrations are such that the structure is localized in a thin slab, the width of which is at most one wavelength, perpendicular to the feeding direction [10, 19]. Such structures may then be considered as quasi-2D.

2. The pattern selection problem

Because reaction–diffusion systems undergoing auto- or cross-catalytic processes are inherently nonlinear one expects the occurrence of some multiplicity in the number of solutions as a result of bifurcation phenomena.

Pattern selection is then, in some sense, the study of the relative stability of, or competition among, these solutions when they are the result of symmetry-breaking bifurcations. More precisely, its aim lies in the determination, for given parametric conditions, of the possible structures – geometrical aspect, orientation, wavelength – and their stability properties. This problem was already on Turing's mind when he stated in the final sections of his paper [1]:

"Most of an organism, most of the time, is developing from one pattern into another, rather than from homogeneity into a pattern. One would like to be able to follow this more general process mathematically also".

The basic equation for the study of Turing structures are reaction–diffusion equations:

$$\frac{\partial \boldsymbol{C}}{\partial t} = \boldsymbol{f}(\boldsymbol{C}) + D\nabla^2 \boldsymbol{C} ,$$

where $\boldsymbol{C}$ is a vector of concentrations, $\boldsymbol{f}(\boldsymbol{C})$ represents the reaction kinetics and D is the diffusion matrix.

Linear stability analysis of the reference uniform state $\boldsymbol{C}_0$ leads in general to a complex dispersion relation for the growth rate $\sigma(\boldsymbol{k}, B)$ and frequency

$\omega(\boldsymbol{k}, B)$ as a function of the wavevector $\boldsymbol{k}$ of the perturbation and control parameter B. From this dispersion relation one determines the critical wavevector $\boldsymbol{k}_c$ corresponding to the lowest value, B_c, of B at which the growth rate σ first becomes positive. Turing's instability corresponds to the class of space-symmetry-breaking instabilities that are characterized by the fact that, at B_c, $\sigma = 0$ occurs with $\omega = 0$ and $k_c \neq 0$. To tackle the problem above B_c, one must first determine which set of modes are active in the leading approximation to the solution of the nonlinear problem.

In small systems, the size of which is of the order of the wavelength $(2\pi/k_c)$ of the emerging pattern, the spectrum of the linearized operator is discrete, and at most finitely degenerate. Thus only a finite number of modes become excited and the concentration field $\boldsymbol{C}(\boldsymbol{r}, t)$ may be approximated by a linear superposition of these modes, which interact nonlinearly. In this case, the center manifold theorem [20] assures that the original reaction–diffusion equations are well approximated by the reduced dynamics represented by a finite set of nonlinear ordinary differential equations – the amplitude equations – that may be derived by standard techniques [2].

No such theorem exists, however, for large systems where the boundaries are at infinity or too far away to constrain the spectrum of spatial modes. It is nevertheless the case we have to consider to address the experimental Turing patterns as they exhibit the characteristics of extended systems. In the present state of the trade, the tackling of a large degeneracy of the linear spectrum is organized along two axes that bear directly on the problem of pattern selection [21, 22].

The first is related to the *geometrical aspect of the pattern* and its *orientation*. Often indeed $\boldsymbol{k}_c$ will not be unique, reflecting some symmetry in the equations or boundary conditions. In the isotropic reaction–diffusion equations, which are the rule in liquid phase, we have a rotational degeneracy because the linear growth rate depends only on the modulus of $\boldsymbol{k}$, $\sigma = \sigma(k^2, B)$, and therefore all modes lying on the sphere (circle in 2D) of radius $|\boldsymbol{k}| = k_c$ may equally become excited and must therefore be included in the analysis. There is at present no completely satisfactory way to treat this problem. To proceed, one allows all the sets $(M = 1, \ldots)$ of pairs of discrete modes $\boldsymbol{k}_i$ $(|\boldsymbol{k}_i| = k_c)$, $i = 1, \ldots M$, to compete with each other and one determines which combination

$$\boldsymbol{C}(\boldsymbol{r}, t) = \boldsymbol{C}_0 + \sum_{i=1}^{M} (A_i \, e^{i\boldsymbol{k}_i \cdot \boldsymbol{r}} + A_i^* \, e^{-i\boldsymbol{k}_i \cdot \boldsymbol{r}}) , \qquad |\boldsymbol{k}_i| = k_c ,$$

will be favored by the nonlinear coupling. It is the combinations of $\boldsymbol{k}_i$ modes that determine the physical aspect of the patterns. They are related to the tessellations of space [23], e.g. in 2D we may have stripes $(M = 1)$, rhombi

($M=2$), triangles ($M=3$), hexagons ($M=3$). The presence of anisotropies tends to partially lift the orientational degeneracy, thereby modifying the pattern selection. For instance, the void lattices in metals subjected to irradiation (a system that may sometimes be cast in the form of a reaction–diffusion problem) are influenced by the symmetry of the underlying host atomic lattice [24, 25]. Similar effects may also come into play in the spatio-temporal structures [26, 27] obtained recently for the catalytic oxidation of CO on Pt [110] [28].

The other effect touches on the *wavelength of the pattern* and can be dealt with in a much more satisfactory way. It is related to the quasi-degeneracy linked with the existence of the finite continuous band of modes, which, as soon as $B > B_c$, become simultaneously unstable with the critical modes $\boldsymbol{k}_i$ ($|\boldsymbol{k}_i| = k_c$), $i = 1, \ldots M$. For a given B, one must thus take into account all the modes that lie inside the neutral stability curves $\sigma(k^2, B) = 0$. In large, finite geometries, although these modes are quantified they are so close together that we may best think of them as a quasi-continuum. The effects of these sidebands of modes is best captured by considering the excitation of wave packets of modes centered on the critical modes.

The full problem naturally takes both aspects into account. Using the standard techniques of bifurcation analysis, one determines the nonlinear complex amplitude equations that arise through asymptotic solvability conditions and that, for a pattern characterized by M pairs of wavevectors ($i = 1, \ldots, M$), are of the form

$$\frac{\partial A_i}{\partial t} = \left[\frac{B - B_c}{B_c} + \left(\frac{\partial}{\partial x_i} - \frac{\mathrm{i}}{2k_c}\frac{\partial^2}{\partial y_i^2}\right)^2\right] A_i + v(B) \sum_j^M \sum_k^M A_j^* A_k^* \delta(\boldsymbol{k}_i + \boldsymbol{k}_j + \boldsymbol{k}_k) - \sum_j^M \gamma_{ij} |A_j|^2 A_i - \sum_j^M \sum_k^M \sum_l^M \beta_{jkl} A_j^* A_k^* A_l^* \delta(\boldsymbol{k}_i + \boldsymbol{k}_j + \boldsymbol{k}_k + \boldsymbol{k}_l) ,$$

where x_i and y_i lie respectively in the directions parallel and orthogonal to $\boldsymbol{k}_i$. The last term represents the contributions of noncoplanar quadrangles of $\boldsymbol{k}_i$ that may arise in 3D. In these partial differential equations the spatial operators take the effect of the sidebands into account and therefore permit the treatment of modulational effects related for instance to the presence of boundaries, defects, ...

It is worthwhile noting that many of the typical nonlinear equations of mathematical physics – Korteweg–de Vries, nonlinear Schrödinger, ... – arise precisely through a similar procedure. They therefore possess universal fea-

tures as their structure is determined solely by the symmetries of the given problem and only the values of the coefficients in the amplitude equation take care of the idiosyncrasies of the specific problem considered. However, this universality is lost as soon as secondary, tertiary, ... bifurcations come into play [29, 30]. One is then led to consider scenarios eventually leading to the spatio-temporal complex phenomena that arise in these large aspect ratio systems with loss of various kinds of correlations and proliferation of defects as was done earlier for the roads to chaos in small systems [22].

In principle, once the amplitude equations, and their coefficients, are known it is possible to study the *stability* of the various structures with different geometrical form and wavelength. When the amplitude equations are relaxational and can thus be derived from a Lyapunov functional $L[A, A^*]$ such that

$$\frac{\partial A_i}{\partial t} = -\frac{\delta L}{\delta A_i^*} \qquad \text{where } \frac{\partial L}{\partial t} = -\sum_i \left(\frac{\delta L}{\delta A_i^*}\right)^2 \leqslant 0 ,$$

the globally stable pattern corresponds, for given B, to the absolute minimum of $L[A, A^*]$, whereas the relative minima represent metastable structures. This simple picture, at best valid near B_c, is soon lost when B increases as most nonlinear problems, and certainly the chemical systems we are interested in, do not exhibit this so-called variational property.

This relative stability problem for variational systems may also be resolved by considering the velocity of a domain wall (front) joining two (stable) solutions of the amplitude equation: If these two structures (say α and β) are bistable between values B_1 and B_2 of the control parameter, there exists one value B_{c0}, for which the wall is stationary (zero velocity), and the phases α and β coexist spatially. For all other values in the interval $\{B_1, B_2\}$ one phase will dominate the other and will invade the whole system as in classical nucleation theory. This method was recently used [31, 32] to study the coexistence of $M = 3$ and $M = 1$ structures in a 2D model. One has then to test for all the relative orientations of the $\boldsymbol{k}_i$ defining both structures with respect to the direction of the domain wall. This problem already complex in itself is even trickier when it puts spatial structures, which possess their own characteristic length $(2\pi/k_c)$, on the stage. In that case so-called nonadiabatic effects describing the pinning of the domain boundaries by the small-scale structure (for instance the concentration cells) seem to play an important role. These exponentially weak effects cannot be accounted for by the amplitude equations that only govern the large-scale modulation of the pattern. Other techniques must then be introduced.

This dynamical method to test the relative stability of two phases is, however, also valid when the system does not present variational properties. It

has so been shown recently that under particular conditions the coexistence point B_{c0} may be shifted by these nonvariational effects leading, in a finite region, to the possibility of stable localized structures [33, 34] (under uniform conditions), the building blocks of which are provided by such domain walls [35–37]. The chemical "flip-flop" [9] recently discovered may fall in this category [38].

In large systems, the particular orientations of the patterns has to be chosen by some external or initial bias, because of the orientational degeneracy. Often, in real experiments, different biases are present in different parts of the domain and a structure with diverse orientations starts growing in various parts of the system. The way in which these orientationally competing patches form compatible patterns is a subject of much present interest. It is not unusual for these patterns to remain time dependent over very long times and indeed never settle down at all. The resulting mismatch leads to the formation of *defects* (dislocations, disclinations) that play an important role in pattern rearrangement. Many aspects of their behaviour may then be described in the framework of phase equations [21, 22].

3. Pattern selection for the Brusselator under uniform conditions

In a distributed system, when written in terms of scaled variables, the Brusselator model [2] is defined by its reaction–diffusion equations

$$\frac{\partial X}{\partial t} = A - (B+1)X + X^2Y + D_X\nabla^2 X\,, \qquad \frac{\partial Y}{\partial t} = BX - X^2Y + D_Y\nabla^2 Y\,,$$

where the concentrations of species A and B serve to control the system, B being specificially chosen as the bifurcation parameter. In this form, A and B are thus taken as pool species that are kept at a constant value in time. In this section that value is also chosen to be uniform over the system. Although rather unrealistic, this so-called pool-chemical approximation lies at the basis of most theoretical developments for the sake of mathematical tractableness. Recent experimental set-ups may however fit into this approximation. The first is that implemented in the already cited new CSTR–membrane reactor [11]. Another situation where this approximation may apply concerns the heterogeneous catalytic reactions [39] over well defined crystalline planes where the feed comes from the gas phase and where spatio-temporal symmetry breaking phenomena on the surface have been reported recently [26–28].

In these conditions, the Brusselator possesses a uniform reference state (thermodynamic branch) $X_0 = A$, $Y_0 = B/A$ that undergoes a space (Turing)

symmetry breaking bifurcation for $B = B_c = (1 + A\sqrt{D_X/D_Y})^2$ with $k_c^2 = A/\sqrt{D_X D_Y}$ when $D_Y > D_X A^2/(\sqrt{1 + A^2} - 1)^2$. This inequality simply implies that the Turing instability takes place before the Hopf bifurcation, which is also supported by the Brusselator. It may be relaxed if one allows, as proposed recently [40], for a fast, reversible reaction involving species X and a slowly diffusing or immobile complexing agent in excess in the system (see fig. 1). This attractive idea may then lie at the basis of a systematic strategy to uncover new Turing structures in chemical systems not related to the CIMA reaction [12].

Because the experimentally obtained structures present the characteristics of large aspect ratio systems, we will not consider Turing patterns in small systems. Their properties are considered for instance in refs. [2, 4].

We now want to summarize our numerical simulations on the Brusselator and put them in relation with the results derived from the nonlinear theory and also the experiments. We essentially used two sets of parameters values:

Set I: $\bar{v} \equiv v(B_c) < 0$, $A = 4.5$, $D_Y/D_X = 8$, $B_c = 6.71$,

Set II: $\bar{v} \equiv v(B_c) > 0$, $A = 2$, $D_Y/D_X = 5$, $B_c = 3.58$,

and the actual values of D_X and D_Y used may be found in the figure captions.

The integrations were carried out on a RISC workstation in order to be able to follow the transient behaviour as well as the asymptotic states. Use was made of an explicit Euler scheme complemented by finite difference methods.

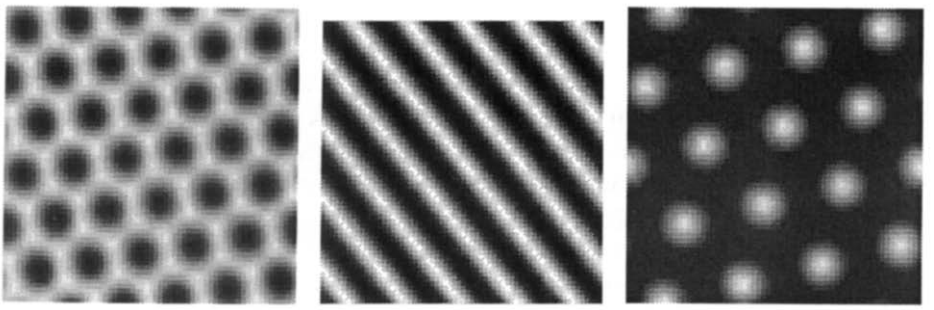

[a] [b] [c]

Fig. 1. The three basic 2D patterns for species X in a Brusselator modified to take the Lengyel–Epstein procedure [40, 12] into account. They are similar to the structures obtained for the standard Brusselator for set I of parameters [55]. The integrations were carried out on a square grid of size 64×64 with periodic boundary conditions. The gray scale corresponds to the concentrations lying between the absolute minimum (black) and maximum (white). They thus measure relative concentration variations. (a) Near critical Hπ ($\bar{v} < 0$) for $A = 1.5$, $D_X = D_Y = 4$, $\sigma = 3$, $B = 6.5$. (b) Stripes for the same set of parameters as in (a) but $B = 7.5$. (c) Near critical H0 ($\bar{v} > 0$) for $A = 0.5$, $D_X = D_Y = 4$, $\sigma = 6$, $B = 3$. Here σ is the complexification factor [40, 12].

3.1. The 3D Brusselator

Using set I, we corroborated [41] the theoretical bifurcation diagram that has been obtained in the weakly nonlinear limit (near B_c) [13, 14, 16]. The following sequence of patterns emerges as B is increased. When the reference state becomes unstable, a body-centered cubic structure ($M = 6$) is the first to appear subcritically. It is followed, also subcritically, by hexagonal prisms ($M = 3$) and then supercritically by lamellae ($M = 1$). As discussed in ref. [9] these patterns may be consistent with the experimentally observed 3D structures. However, more experimental and theoretical work is necessary to make a definite assessment.

3.2. The 2D Brusselator

Because we wanted to test the effects of ramps that extend to values of B beyond the range of validity of the weakly nonlinear theory, we analyzed the 2D pattern selection more thoroughly. This part of our work is complementary to that undertaken by Dufiet and Boissonade [42, 43] for the Schnackenberg model [44].

3.2.1. Near B_c

When $\bar{v} < 0$, a structure of hexagonal symmetry is first obtained, on increasing B quasistatically, where the maxima of concentration of X are arranged on a honeycomb lattice (Hπ structure – $M = 3$) (fig. 1a). Further, these Hπ become unstable with respect to stripes ($M = 1$) (fig. 1b). Reversing the variation of B allows to recover the Hπ but by undergoing an hysteresis loop (insert of fig. 2).

In this range we thus recover the sequence of events predicted by the weakly nonlinear theory [13–18], i.e. the standard hexagons-"rolls" competition known from the Rayleigh–Bénard [23, 45–48] and the Bénard–Marangoni [49] problems. It is therefore not totally surprising that stripes and hexagons have also been observed [10–12] in some of the experimental work to date of Turing structures.

When $\bar{v} > 0$, the first structure of hexagonal symmetry now gives rise to maxima of X concentration forming a triangular lattice (H0 structure – $M = 3$) (fig. 1c).

In an unbounded system the stripes are determined up to a phase factor that corresponds to the fact that an arbitrary translation leaves the pattern invariant. However, the patterns with hexagonal symmetry are composed of three sets of stripes and two phases are sufficient to describe all the translations in the plane. The third phase or equivalently the sum of the three phases must thus be determined by the dynamics. The Hπ and H0 patterns therefore differ

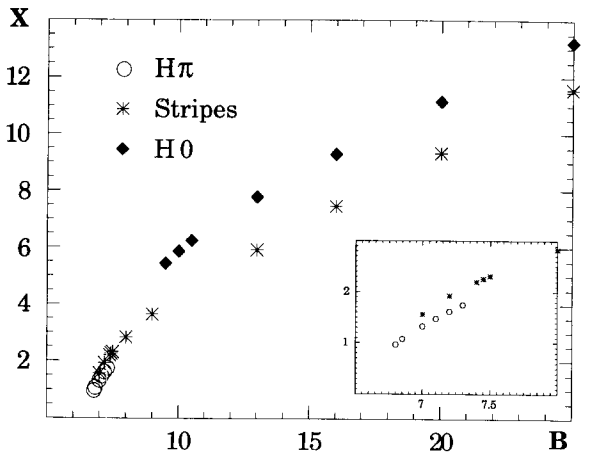

Fig. 2. Bifurcation diagram compiled from the numerical simulations using set I of parameters. $[X_{max} - X_0]$ is drawn as a function of the bifurcation parameter B. The inset zooms in the region near B_c.

only by the value of the sum of the phases that is recalled in the notation used.

It is remarkable that for different kinetics, or smaller size systems and even for other boundary forms or conditions the same 2D (and probably 3D) patterns should emerge [42, 43, 50–53]. This may bring some light to the understanding of the patterns obtained in a capillary [54].

3.2.2. Reentrant hexagons

When $\bar{v} < 0$, starting on the previously described stripe branch and increasing B again quasistatically, the stripes eventually become unstable with respect to an H0 type pattern (fig. 2). These remain stable for still higher values of B (this was tested up to $B = 32$). At this point, decreasing B again leads back to the stripes with the appearance of another hysteresis loop. The previous loop and this one were never seen to overlap for the parameters values that we screened. Such a reentrant hexagonal phase was also discovered by Dufiet and Boissonade [42, 43].

When $\bar{v} > 0$, the situation is different. Indeed the H0, obtained in this case near B_c, never destabilized to stripes (that may however appear as an isolated branch) or another Hπ structure when increasing B quasistatically. The secondary bifurcations therefore really lead to the breakdown of the simple universality that prevails near B_c.

These scenarios, for the Brusselator and the Schnackenberg models, can be explained simply in terms of a renormalization, due to higher-order nonlinear contributions, of the quadratic coupling coefficient v [55, 56]. The two kinds of

hexagons have been observed (see fig. 3a,b of ref. [57]), one of them being only transitorily. However, a stationary succession Hπ/stripes/H0 may have been seen experimentally in the presence of gradients [19]. Indeed as will be seen in section 4 the presence of a ramp permits the unfolding in space of the bifurcation diagram (spatial coexistence).

3.2.3. *Zig-zag patterns*

A branch of zig-zag stripes (fig. 3) simultaneously stable with the straight stripes was also uncovered when starting from random initial conditions instead of proceeding quasistatically from the Hπ. Such patterns arise also in the electrohydrodynamic instabilities of a nematic liquid crystal [58]. When B increases, the knee angle in the structure also grows steadily (fig. 4) until it hits $\pi/6$ where the zig-zag pattern becomes unstable to the H0 structure.

Standard stability analysis [22] implies that in the $k < k_c$ sideband stripes undergo a zig-zag instability inducing a periodic modulation of the concentration field in the direction of the axis of the stripes. It was shown recently [59, 60] that this instability may saturate for $k \leqslant k_c$ giving rise to zig-zag stripes whereas for deeper quenches in the sideband no saturation of the zig-zag mode occurs and the zigs and zags of successive stripes reconnect to yield a new set of straight stripes. Both these processes have also been observed by Dufiet and Boissonade [42]. Such wavy stripes were also obtained for the hyperchirality model [52]. For other conditions the zig-zag instability may also give rise to the creation of defects and chaos [60].

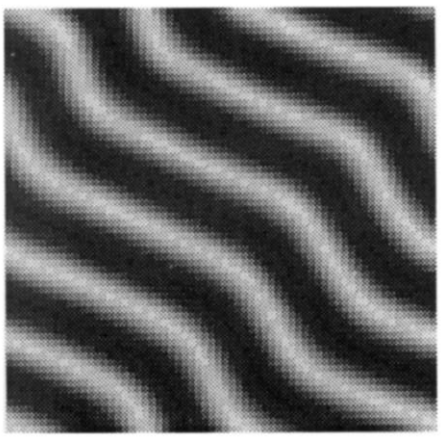

Fig. 3. Zig-zag stripes on a 64×64 grid with periodic boundary conditions with set I of parameters for $D_X = 7$ and $B = 10$.

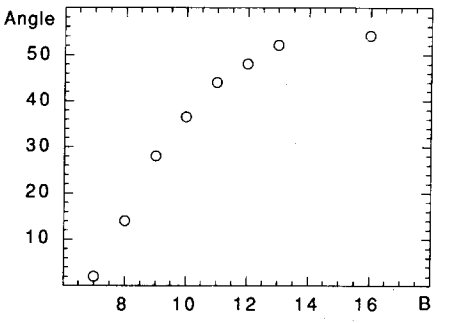

Fig. 4. Bifurcation diagram representing the size of the knee angle of the zig-zig stripes as a function of B for set I of parameters.

Such undulated stripes have not been seen experimentally but then in the large aspect ratios of the experiments they may be hard to untangle from a straight stripes domain invaded by disclinations and dislocations [10–12]. Indeed as mentioned in section 2 in large systems defects come into play and are not necessarily eliminated by the dynamics. A large aspect ratio Hπ structure (fig. 5) contains numerous defects, in this case pentagonal–heptagonal pairs, which separate well ordered domains. Once the amplitude has saturated, the remaining dynamics consists only of the slow drift of these defects. It is reminiscent of some experimental observations [10, 57].

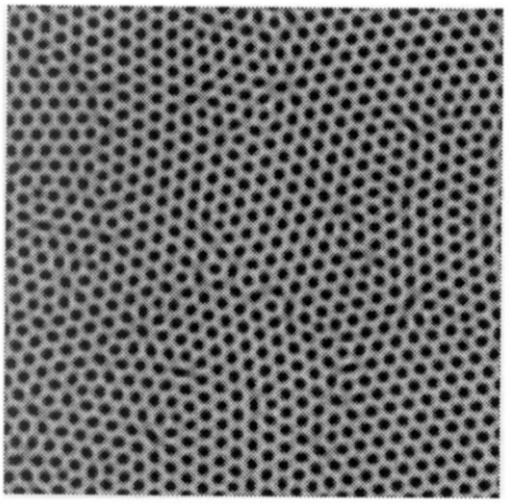

Fig. 5. Hexagonal pattern (Hπ) for the concentration of species X of the standard Brusselator in a large system (256×256) with periodic boundary conditions and $A = 4.5$, $B = 7.1$, $D_X = 2.8$, $D_Y = 22.4$.

4. Pattern selection for the ramped Brusselator

Selection in the presence of ramps has previously been studied to take into account the effects of small experimental imperfections in hydrodynamical problems even though researchers in that field often appeal to reaction–diffusion systems, which are more tractable than the equations of fluid mechanics. One thoroughly studied problem is related to wavelength selection inside the sideband degenerate states. If the control parameter varies in space, such that it becomes subcritical in part of the system then the stable band is reduced and – in the limit of infinitely slow variation – shrinks to a single wavenumber. The wavelength is then perfectly selected [61]. It was further shown that the selected solution need not be stationary, leading eventually to oscillations or even chaotic behaviour [62]. Some of these results were verified experimentally for the Taylor vortex flow [63]. Theoretical analyses were also undertaken for the Rayleigh–Bénard convection problem when the heating is weakly nonuniform [64–67]. Here the lack of experimental results does however not permit to draw definitive conclusions. The effects of some type of ramps were also considered in nonlinear chemical systems. We return to these below.

Our aim in this section is to show, with the aid of a few numerical experiments, how the pattern selection may be affected by the variations in space of the parameters, for instance the bifurcation parameter. Understandingly pattern selection theory is much less developed under nonuniform conditions. The results presented here must thus be considered as first steps in the search for the occurrence of generic behaviours permitting to disentangle the various contradictory orientational effects that are at play in the presence of ramps. Therefore most questions we raise will go unanswered.

The simplest principle that springs to the mind is that a pattern will develop in the region of space where the local value of the bifurcation parameter allows it to be stable in the corresponding uniform problem. We will however see that even such a simple idea is not always true. It also leads immediately to the prediction of spatial coexistence of structures with different symmetries and a possible high order multiplicity, resulting from multistability, among various different spatial coexistences. The orientational role of the slope of the profile, domain walls and boundaries are furthermore difficult to assess.

Here again we appeal to the pool approximation: the concentrations of A and B are kept constant in time but are given specific profiles. We will make use of linear (where the direction of the gradient is denoted by $\boldsymbol{G}$) and chain-like ramps.

4.1. *Linear ramps*

Linear ramps in the reaction–diffusion context were previously mainly

considered in relation to polarity effects in problems with a biological content [51, 53, 68]. Recently crossed linear ramps on two pool species where studied numerically [69] in the context of the new Turing experiments.

4.1.1. 3D Brusselator

In relation with the experimental results some simulations were carried out for set I of parameters in parallelepipeds.

If, as for the Bordeaux reactor type geometry, the ramp is applied along one of the large sides of the gel slab, we obtain numerically the spatial coexistence of the three kinds of patterns we described in section 3: bcc, hex prisms ($\boldsymbol{k}_1 + \boldsymbol{k}_2 + \boldsymbol{k}_3 = \boldsymbol{0}$, all $\boldsymbol{k}_i \perp \boldsymbol{G}$) and lamellae ($\boldsymbol{k}_1 \perp \boldsymbol{G}$) in order of increasing value of B along the ramp (see fig. 5 of ref. [70]). The transition regions (domain walls) between the coexisting 3D patterns are however very complex and a systematic study of their relative orientations will require to switch to more powerful numerical means to be able to control size and boundary effects.

4.1.2. 2D Brusselator

All our 2D numerical experiments were made with set I parameters on a grid of size L, in the direction of the gradient, times L'. The ramp is applied to the bifurcation parameter B that varies along L: its value is B_L at L and we apply $B = B_c$ at grid points $(\frac{1}{3}L, y)$ in order to define a subcritical region. No flux boundary conditions are imposed along the sides perpendicular to the ramp and periodic boundary conditions along the others.

Let us start by presenting (fig. 6) a typical result. In this case the simple argument alluded to above is true and three regions are visible at a glance: transverse stripes at the highest B values with wavevector $\boldsymbol{k}_s // \boldsymbol{G}$, H$\pi$ with wavevectors $\boldsymbol{k}_1 \perp \boldsymbol{G}$ ($\boldsymbol{k}_1 + \boldsymbol{k}_2 + \boldsymbol{k}_3 = \boldsymbol{0}$) near B_c, which invade the subcritical region. There is also a domain wall between Hπ and stripes. In the region straddling B_c, we find the amplitude variations characteristic of *imperfect bifurcations*, here to an hexagonal phase. Such bifurcations have only been studied theoretically in the present context for $M = 1$ structures in weak linear ramps [65, 67]. While the unfolding of patterns (spatial succession of Hπ and stripes) is trivial, the influence of the ramp, the boundaries (they induce a forcing because in general the ramped reference state does not satisfy the imposed boundary conditions) and the existing domain wall on their orientation (for instance the relative orientation of $\boldsymbol{k}_1$ to $\boldsymbol{k}_s$) lies at the heart of the pattern selection problem. To deepen the plot let us dissect two numerical experiments.

Experiment A (*fig. 7*). The conditions are the same as those just discussed. We start at $B_L = 7$ with random initial conditions. This leads to the pattern

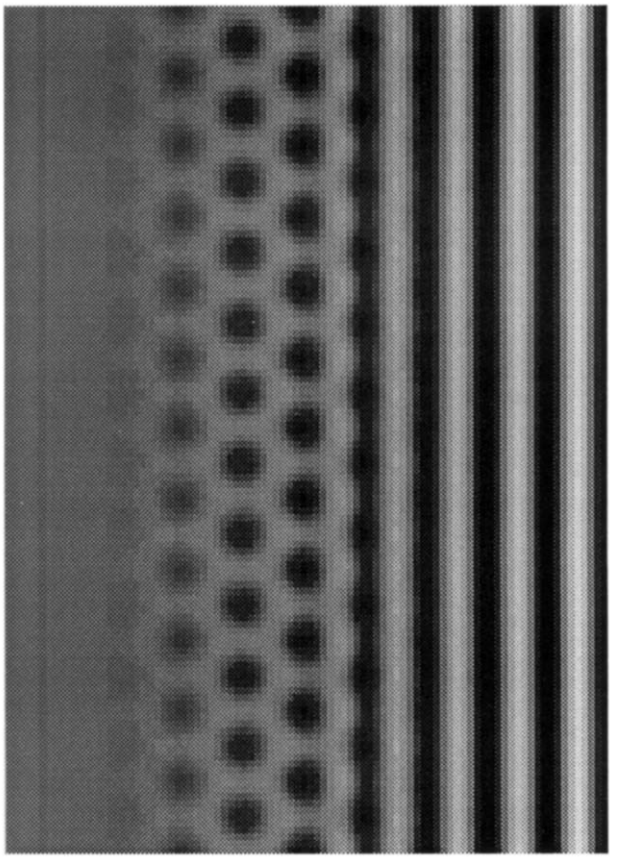

Fig. 6. Typical spatial coexistence of Hπ and transverse stripes resulting from the existence of a linear ramp from the left to the right. Set I of parameters, with $D_X = 3.5$, have been used on a 90×128 ($L \times L'$) grid. Here $B_L = 8$ while $B = B_c = 6.71$ is imposed at grid points $(30, y)$. Boundary conditions are no-flux to the left and right and periodic at top and bottom.

shown in (fig. 7a). There is nothing particular to witness. We have only the Hπ (oriented as before) because B_L is still below the lower stability limit of stripes in the uniform system. We then proceed by making a series of quasistatical modifications of B_L. When $B_L = 8$ (fig. 7b) we still have only Hπ, even though near grid point L we are, for uniform systems, in a region where the Hπ are unstable. So our simple principle is already failing us: the ramp has broadened the stability domain of the Hπ. Contrary to what we saw above transverse stripes do not occur and the Hπ even have to incur some deformation to fit in the system for these conditions. Increasing again B_L to 8.2 (fig. 7c), the situation changes radically: the Hπ snap back to their uniform equivalent stability region but the stripes that enter the show appear with $\boldsymbol{k}_s \| \boldsymbol{k}_2$ (or $\boldsymbol{k}_3$)

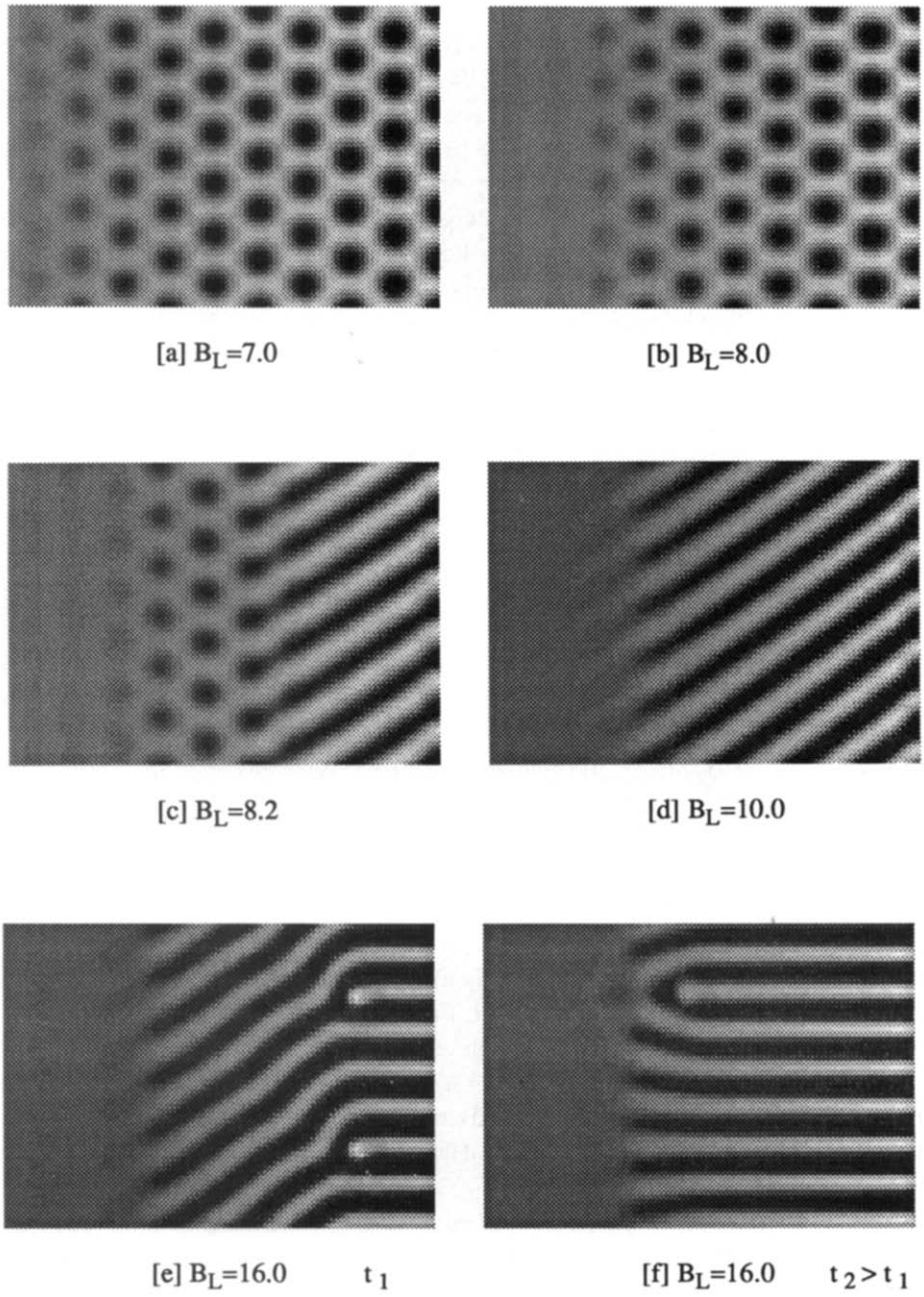

Fig. 7. Experiment A for the same conditions as in the previous figure on a grid of size 90×64. (a) $B_L = 7$; (b) $B_L = 8$; (c) $B_L = 8.2$; (d) $B_L = 10$; (e) and (f) $B_L = 16$ at two successive times. Pattern (a) is obtained from random initial conditions and all the others by increasing B_L quasistatically from the preceding stationary one.

implying an orientational effect of the domain wall. The only influence of the L boundary is a slight bend of the stripes to meet the no flux boundary condition. Furthermore the new oblique stripes (with respect to $\boldsymbol{G}$) are drifting perpendicularly to $\boldsymbol{G}$ at constant velocity (on the way up or down depending on whether $\boldsymbol{k}_s \| \boldsymbol{k}_2$ or $\boldsymbol{k}_3$) because of the presence of periodic boundaries in that direction. This is the sign that a parity-breaking bifurcation [71] with respect to the direction of the gradient has occurred. The Hπ are entrained in the process. For $B_L = 10$ (fig. 7d), while the whole structure continues its motion, the Hπ are in the process of being squeezed out because the gradient is now so large that they have less than one wavelength to fit into. As soon as the Hπ have vanished a set of longitudinal stripes starts to invade the system spontaneously from the L border. These new stripes eventually invade the whole supercritical region (fig. 7e,f). No H0 intervene yet because of the quasistatical nature of the procedure.

Experiment B. The conditions are again the same but at each increase of B_L we start from random initial conditions. For $B_L = 8$ we have the pattern (fig. 6) discussed at length before. Having in mind the result of experiment A for the same values of the parameters, we here observe a clear-cut example of bistability between a state exhibiting only Hπ and another state that unfolds both Hπ and transverse stripes. On increasing the ramp the stripes invade more and more of the system until, as before, the Hπ are expelled and only transverse stripes remain. The selection of stripes over Hπ in these ramps does not seem to be the result of a simple kind of anisotropic effect favoring $M = 1$ structures over $M = 3$ patterns [72] because at $B_L = 14$ the H0 have been allowed to come into play. Furthermore, as soon as the H0 appear, necessarily near B_L, the transverse "bulk" stripes seem to be screened from the B_L boundary by these H0 (remarkably a lonely transverse stripe is present near B_L). They then start to bend, probably aided by the presence of zig-zag stripes that are present also in the region of B. Finally, after a long transient we obtain the pattern of fig. 8 for $B_L = 16$, which exhibits the coexistence of longitudinal stripes ($\boldsymbol{k}_s \perp \boldsymbol{G}$), H0 ($\boldsymbol{k}_1 \perp \boldsymbol{G}$, $\boldsymbol{k}_1 + \boldsymbol{k}_2 + \boldsymbol{k}_3 = \boldsymbol{0}$) and still the lonely transverse stripe ($\boldsymbol{k}_s \| \boldsymbol{G}$). The H0 are observed to present the same orientation with respect to the gradient as the former Hπ.

Let us remark that many numerical experiments with ramps lead to patterns containing a lot of bend stripes and defects probably because of the ubiquitous use of zig-zag stripes that are stable for a wide range of values of B. This leads to a further increase of the multiplicity of possible structures. Furthermore as soon as a region contains stripes oblique to $\boldsymbol{G}$ a drift of the whole structure comes into play.

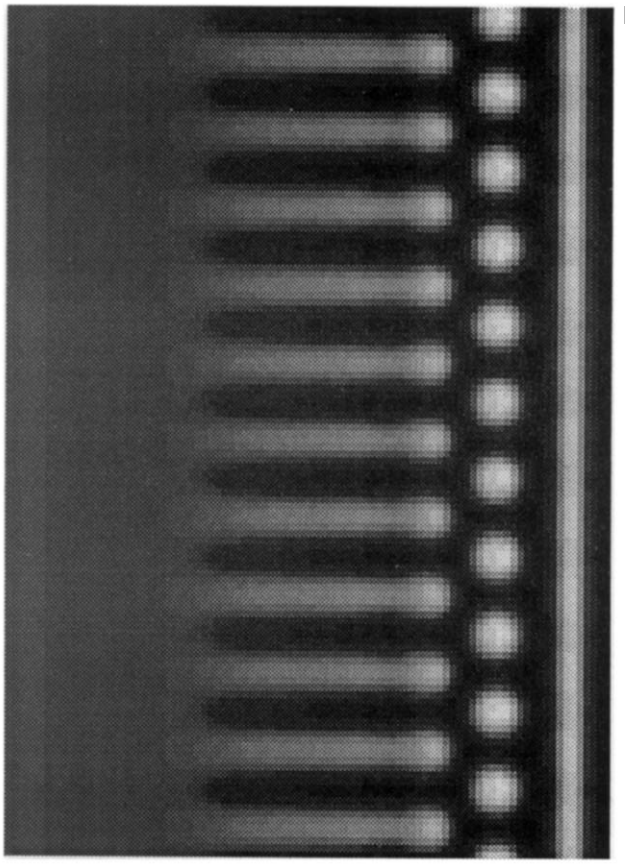

Fig. 8. Final pattern in the sequence of events for experiment B described in the text. For this particular pattern set I is used with $D_X = 7$ for a 90×128 grid with the same boundary conditions as before. $B_L = 16$. It exhibits the coexistence in the ramp of longitudinal stripes, H0 and a single transverse stripe.

So one starts to understand that the pattern selection becomes indeed very complicated, even in the presence of the simplest form of profile. Considering only the stripes, we have seen, as was already the case for the nonuniformly heated Rayleigh–Bénard problem, that the slope of the ramp and the boundaries (and in our case also the wall boundaries) conspire to determine the selected orientation. Other experiments with linear ramps will be presented elsewhere [73].

4.2. *Chain-like ramps*

These were considered before both theoretically [74, 2] and numerically [75, 2] for 1D chemical systems because such ramps are the kind of spatial

dispersion one gets for the A species in the Brusselator if it is let free to diffuse from the boundaries. The effects of similar ramps in the nonuniformly heated Rayleigh–Bénard convection problem were also assessed [64, 66].

It was shown that such profiles give rise to localized structures (not to be confused with those considered in section 2, which appear under uniform conditions): the structure determines the extent of its own region of existence and within this region, as for linear ramps, spatial coexistence of patterns of different symmetries is possible. For these ramps, the *bifurcations* are however *perfect* [76] but are delayed, with respect to the uniform conditions, because the bifurcation parameter must be sufficiently large that one wavelength of the structure may fit in the supercritical region for Hπ or transverse stripes. For longitudinal stripes, which are the first to appear because they are not sensitive to such a restriction on the width of the supercritical region, the curvature of the profile near threshold nevertheless also delays the bifurcation [77]. Some illustrations are given in figs. 9 and 10. It is also worthwhile noting that the H0 (fig. 9) are oriented differently from the linear ramp case.

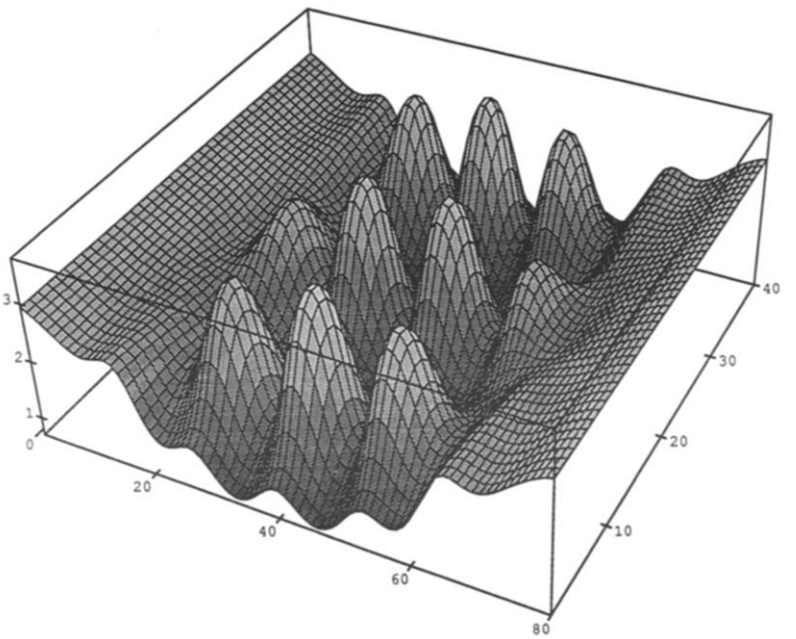

Fig. 9. 3D amplitude plot for the concentration of species X in the Brusselator in the presence of a symmetric chain-like ramp of A resulting from its diffusion from the boundaries ($D_A = 12$) in the presence of a linear consumption with constant $k_A = 0.01$. The size of the grid is 80×40 and B is maintained at the uniform value 3.7. On the lateral sides we impose concentrations: $A(0) = 3$, $X(0) = A(0)$, $Y(0) = B/A(0)$. We use periodic boundary conditions along the other sides. $D_X = 4$, $D_Y = 20$. As initial condition we take $X = A(x)$ and $Y = B/A(x)$ and apply a small sinusoidal perturbation parallelly to the ramp.

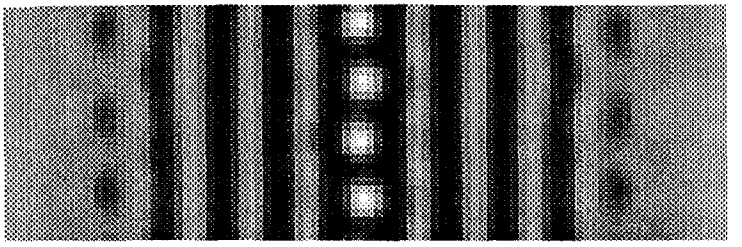

Fig. 10. Coexistence of Hπ (near the lateral walls), stripes and H0 in the presence of a symmetric chain-like ramp of A and for conditions similar to fig. 9. Here $D_A = 10$, $k_A = 0.01$, $A(0) = 10$, $D_X = 3.5$, $D_Y = 28$ and $B = 12$. The grid size is 90×30. The initial condition is also similar but the perturbation consists in multiplying the concentration of X(45, y) by a factor of two.

5. Conclusions

It should by now be clear that the study of Turing structures presents new challenges to pattern selection theory: characterization of the first genuine 3D periodic patterns in far from equilibrium conditions and of the stability of 2D polygonal structures, which may complement the information obtained from hydrodynamical systems. The incorporation of the effects of profiles of the control parameters, which derive naturally from the experimental context, introduce further difficulties.

But already new incitements, linked to the Turing patterns, are brought to us by the experimentalists. They are related to the reappearance of the time dependance one had tried to ward off as for instance with the help of the Lengyel–Epstein procedure [40, 12]. The first of these new teasers, dubbed "chemical turbulence" for lack of better wording, manifests [56] itself as a new time dependent phase with proliferation of defects that, for some conditions, squeeze in between the stripes and the hexagons. The other, christened "chemical flip-flop" [9] is a localized asymmetric emitter, a chemical beacon, which, thanks to the ramps, lives in a quasi-1D world in a region of experimental parameters where Turing and Hopf instabilities interact. Both have in common that they point once more to the complex wonders that remain to be discovered in our nonlinear chemical playground.

Acknowledgements

We thank G. Nicolis for his interest in this work and A. Arneodo, J. Boissonade, P. De Kepper, S. Metens, Q. Ouyang and H. Swinney for stimulating discussions and for communicating results prior to publication. This

work was sponsored by Twinning contract #SC1*-CT91-0706(TSTS) of the EC Science Program.

References

[1] A. Turing, Philos. Trans. R. Soc. Lond. B 237 (1952) 37.
[2] G. Nicolis and I. Prigogine, Self-Organization in Nonequilibrium Systems (Wiley, New York, 1977).
[3] H. Meinhardt, Models of Biological Pattern Formation (Academic Press, New York, 1982).
[4] J.D. Murray, Mathematical Biology (Springer, Berlin, 1989).
[5] P.W. Anderson, in: Order and Fluctuations in Equilibrium and Nonequilibrium Statistical Mechanics, G. Nicolis, G. Dewel and J.W. Turner, eds. (Wiley, New York, 1981) p. 289.
[6] D. Walgraef, G. Dewel and P. Borckmans, J. Chem. Phys. 74 (1981) 755.
[7] V. Castets, E. Dulos, J. Boissonade and P. De Kepper, Phys. Rev. Lett. 64 (1990) 2953.
[8] P. De Kepper, V. Castets, E. Dulos and J. Boissonade, Physica D 49 (1991) 16.
[9] J.J. Perraud, K. Agladze, E. Dulos and P. De Kepper, Physica A 188 (1992) 1, this Workshop.
[10] Q. Ouyang and H. Swinney, Nature 352 (1991) 610.
[11] R.D. Vigil, Q. Ouyang and H. Swinney, Physica A 188 (1992) 17, this Workshop.
[12] I.R. Epstein, I. Lengyel, S. Kádár, M. Kagan and M. Yokoyama, Physica A 188 (1992) 26, this Workshop.
[13] G. Dewel, P. Borckmans and D. Walgraef, J. Phys. C 12 (1979) L491.
[14] D. Walgraef, G. Dewel and P. Borckmans, Phys. Rev. A 21 (1980) 397.
[15] L.M. Pismen, J. Chem. Phys. 72 (1980) 1900.
[16] D. Walgraef, G. Dewel and P. Borckmans, Adv. Chem. Phys. 49 (1982) 311.
[17] A. Nitzan and P. Ortoleva, Phys. Rev. A 21 (1980) 1735.
[18] H. Haken and H. Olbrich, J. Math. Biol. 317 (1978).
[19] Q. Ouyang, Z. Noszticzius and H. Swinney, Spatial bistability of two-dimensional Turing patterns in a reaction–diffusion system, preprint (1992).
[20] J. Guckenheimer and P. Holmes, Nonlinear Oscillations, Dynamical Systems, and bifurcations of Vector Fields (Springer, Berlin, 1983).
[21] A.C. Newell, in: Complex Systems, D. Stein, ed. (Addison–Wesley, Longman, 1989) p. 107.
[22] P. Manneville, Dissipative Structures and Weak Turbulence (Academic Press, Boston, 1990).
[23] F.H. Busse, Rep. Prog. Phys. 41 (1978) 1929.
[24] K. Krishan, Nature 287 (1980) 420.
[25] D. Walgraef and N.M. Ghoniem, Phys. Rev. B 39 (1989) 8867.
[26] J. Falta, R. Imbihl and M. Henzler, Phys. Rev. Lett. 64 (1990) 1409.
[27] S. Jakubith, H. Rothermund, W. Engel, A. von Oertzen and G. Ertl, Phys. Rev. Lett. 65 (1990) 3013.
[28] G. Ertl, Science 254 (1991) 1750.
[29] G. Nicolis, T. Erneux and M. Herschkowitz-Kaufman, Adv. Chem. Phys. 38 (1978) 263.
[30] P. Coullet and G. Iooss, Phys. Rev. Lett. 64 (1990) 866.
[31] Y. Pomeau, Physica D 23 (1986) 3.
[32] B.A. Malomed, A.A. Nepomnyaschy and M.I. Tribelsky, Phys. Rev. A 42 (1990) 7244.
[33] S. Koga and Y. Kuramoto, Prog. Theor. Phys. 63 (1980) 106.
[34] O. Thual and S. Fauve, J. Phys. (Paris) 49 (1988) 1829.
[35] S. Fauve and O. Thual, Phys. Rev. Lett. 64 (1990) 282.
[36] V. Hakim, P. Jakobsen and Y. Pomeau, Europhys. Lett. 11 (1990) 19.
[37] W. Van Saarloos and P.C. Hohenberg, Phys. Rev. Lett. 64 (1990) 749.

[38] G. Dewel and P. Borckmans, in: Solitons and Chaos, I. Antoniou and F. Lambert, eds., Springer Research Reports in Physics (Springer, Berlin, 1991) p. 138.
[39] R. Aris, Lect. Appl. Math. 24 (1986) 24.
[40] I. Lengyel and I.R. Epstein, Proc. Natl. Acad. Sci. (1992), to appear.
[41] A. De Wit, G. Dewel, P. Borckmans and D. Walgraef, Three-dimensional dissipative structures in reaction–diffusion systems, in: Proc. NATO ARW New Trends in Nonlinear Dynamics: Nonvariational Aspects, C. Pérez-García, ed., Physica D (1992), to appear.
[42] V. Dufiet and J. Boissonade, J. Chem. Phys. 96 (1992) 664.
[43] V. Dufiet and J. Boissonade, Physica A 188 (1992) 158, this Workshop.
[44] J. Schnackenberg, J. Theor. Biol. 81 (1979) 389.
[45] M. Dubois, P. Bergé and J. Wesfreid, J. Phys. (Paris) 39 (1978) 1253.
[46] S. Ciliberto, E. Pampaloni and C. Perez-Garcia, Phys. Rev. Lett. 61 (1988) 1198.
[47] C.W. Meyer, D.S. Cannell and G. Ahlers, Hexagonal and roll flow patterns in temporally modulated Rayleigh–Bénard convection, preprint.
[48] E. Bodenschatz, J. de Bruyn, G. Ahlers and D.S. Cannell, Phys. Rev. Lett. 67 (1991) 3078.
[49] P. Cerisier, C. Jamond, J. Pantaloni and C. Perez-Garcia, Phys. Fluids 30 (1987) 954.
[50] B. Bunow, J.-P. Kernevez, G. Joly and D. Thomas, J. Theor. Biol. 84 (1980) 629.
[51] T.C. Lacalli, D.A. Wilkinson and L.C. Harrison, Development 104 (1988) 105.
[52] M.J. Lyons and L.G. Harrison, Chem. Phys. Lett. 183 (1991) 158.
[53] A. Hunding, Physica A 188 (1992) 172, this Workshop.
[54] K. Agladze, E. Dulos and P. De Kepper, J. Phys. Chem. 96 (1992) 2400.
[55] J. Verdasca, A. De Wit, G. Dewel and P. Borckmans, Phys. Lett. A 168 (1992) 194.
[56] S. Metens, G. Dewel and P. Borckmans, in preparation.
[57] Q. Ouyang and H.L. Swinney, Chaos 1 (1991) 411.
[58] R. Ribotta, A. Joets and Lin Lei, Phys. Rev. Lett. 56 (1986) 1595.
[59] H. Sakaguchi, Prog. Theor. Phys. 86 (1991) 759.
[60] S. Sasa, Prog. Theor. Phys. 84 (1990) 1009.
[61] L. Kramer, E. Ben-Jacob, H. Brand and M.C. Cross, Phys. Rev. Lett. 49 (1982) 1891.
[62] H. Riecke and H. Paape, Europhys. Lett. 14 (1991) 433.
[63] G. Ahlers, Physica D 51 (1991) 421.
[64] P.M. Eagles, Proc. R. Soc. Lond. A 371 (1980) 359.
[65] I.C. Walton, Stud. Appl. Math. 67 (1982) 199.
[66] I.C. Walton, J. Mech. Appl. Math. 35 (1982) 33.
[67] I.C. Walton, J. Fluid, Mech. 131 (1983) 455.
[68] A. Hunding and M. Brøns, Physica D 44 (1990) 285.
[69] J. Boissonade, V. Castets, E. Dulos and P. De Kepper, in: ISNM 97 (Birkhäuser, Basel, 1991) p. 67.
[70] P. Borckmans, G. Dewel, A. De Wit and D. Walgraef, Entropie 164/165 (1991) 83.
[71] P. Coullet, R.E. Goldstein and G.H. Gunaratne, Phys. Rev. Lett. 63 (1989) 1954.
[72] D. Walgraef and C. Schiller, Physica D 27 (1987) 423.
[73] A. De Wit, P. Borckmans and G. Dewel, Turing structures in the presence of gradients, in: Instabilities and Nonequilibrium Structures IV, E. Tirapegui, ed. (Kluwer, Dordrecht, 1992), to appear.
[74] J.F. Auchmuty and G. Nicolis, Bull. Math. Biol. 37 (1975) 323.
[75] M. Herschkowitz-Kaufman and G. Nicolis, J. Chem. Phys. 56 (1972) 1890.
[76] J. Boissonade, J. Phys. (Paris) 49 (1988) 541.
[77] G. Dewel and P. Borckmans, Phys. Lett. A 138 (1989) 189.